Propagation Modeling in an Indoor Environment at Sub-THz Frequencies Based on Ray Tracing

Nektarios Moraitis, and Konstantina S. Nikita
Mobile Radiocommunications Laboratory, National Technical University of Athens and Institute of Communication and Computer Systems, Athens, Greece, morai@mobile.ntua.gr

***Abstract*—This paper presents extensive deterministic simulations in an indoor environment at sub-THz frequencies. All the relative wideband parameters of the channel are determined and assessed, including the time delay and spatial characteristics. It is demonstrated that simulations with an accurate description of the materials and representation of the propagation environment produce reliable results, given the fact that the parameters, obtained from the simulation study, are found to be consistent with measurement results that exist in the literature for similar indoor locations. The root-mean-square delay spread exhibits values in the range of 0.6-5.4 ns and 1.7-23.0 ns, for line-of-sight (LOS) and non-line-of-sight (NLOS) conditions, respectively. A multi-cluster model characterizes very well the power delay profiles of the indoor channel, which are found to be formed by 3 up to 4, and 5 up to 7 cluster groups for LOS and NLOS conditions, respectively. All the relative clusters and ray's decay patterns, as well as their inter-arrival times are also evaluated.**

***Index Terms*—channel characterization, deterministic simulations, indoor propagation, sub-Terahertz.**

I. Introduction

The advent of the sixth generation (6G) wireless networks will present innovative services and applications to the users, extending from accurate localization and wireless cognition, to real-time sensing, augmented reality, and holographic communications [1]. Future wireless communications also foresee ultra-high user densities, ultra-low latencies and throughputs up to Tb/s [2]. The current spectrum allocations are limited in sub-6 GHz band, and at 28 and 60 GHz, being insufficient to meet the requirements of the 6G wireless networks [3]. In this context, researchers have been focused on exploiting sub-THz frequencies where massive spectrum swaths are available that can efficiently support those stringent spectrum demands [4]. The D-band window (110-170 GHz) has been introduced as an attractive option to accommodate spectrum-demanding applications, offering a wide spectrum of 60 GHz [5].

Channel propagation above 100 GHz is very challenging and is expected that short-range links be established. Materials at sub-THz frequencies present high reflectivity, thus inducing high multipath [5], [6]. Furthermore, indoor environments, which are characterized by complexity with various material types, necessitate a rigorous analysis and study of the propagation channel. The atmospheric absorption in D-band is low with a specific attenuation is below 2 dB/km [4]. As a result, excess losses are insignificant and can be neglected in indoor wireless links.

Experimental results at D-band in an indoor environment were initially presented in [1], [4] where path loss results and material characteristics in indoor office locations were assessed at 140 GHz and compared with 28 and 73 GHz. The path loss, the material properties, and the wideband channel characteristics at D-band regarding indoor environments have been measured in [5]-[12]; relative parameters have been assessed such as the time delay and the angular spread of the channel. However, there are limited research attempts that model the power delay profile (PDP) characteristics of the indoor channel at D-band [7], [12].

This article presents an indoor propagation study, where the channel is deterministically evaluated at 140 GHz for line-of-sight (LOS) and non-line-of-sight (NLOS) locations in a conference room, laboratory, and corridor. By performing extensive ray-tracing simulations, the delay and angular parameters of the channel are assessed, along with the *K*-factor that conveys a measure of the channels' sparsity. Furthermore, the simulated wideband channel is modeled in a simple multi-clustered form, and all the relative attributes are delivered, including the ray's and cluster's arrival times, as well as their decay factors.

The introduced features are compared and validated with measured parameters (where available), for similar indoor scenarios that exist in the literature. Similar simulations for indoor scenarios were also introduced in [13], where the channel was characterized based on a multi-ray model. The produced time delay parameters were validated with measured values found in the existing literature at 60 GHz, 300 GHz, and 1 THz. Software-based simulations at 150 GHz, using ray-tracing techniques, were presented in [14], for outdoor locations. However, the delivered results were not validated against measurements. This work aims at providing a simulation-based model of the wideband sub-THz channel, and in contrast to the measurement-based models in [7], [12], demonstrates that simulations with an accurate description of the materials, and representation of the propagation environment, can deliver solid and reliable results that approximate the existing measurement-based parameters.

The rest of this article is organized as follows. The deterministic-based simulations, as well as the indoor environment are described in Section II. The statistical analysis and the parameters of the wideband channel are introduced and discussed in Section III. The modeling of the indoor PDPs and their related features are presented in Section IV, followed by conclusions in Section V.

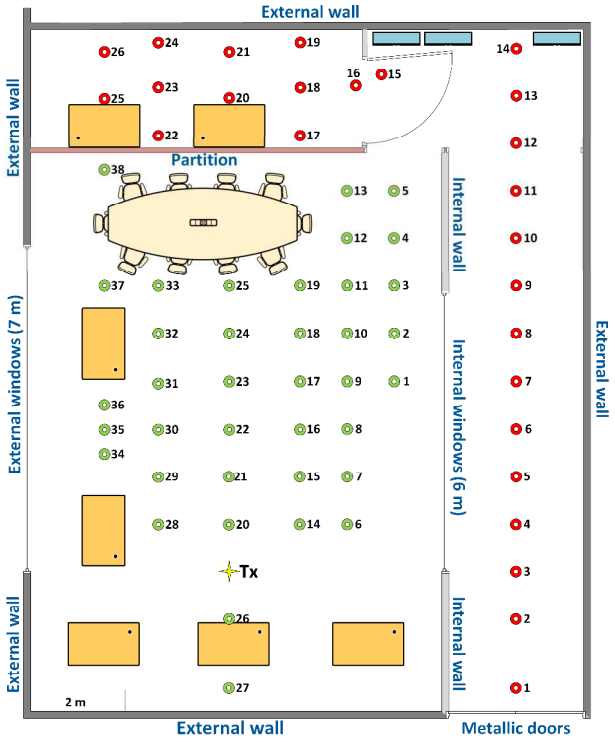

Fig. 1. Scaled ground plan of the indoor environment.

II. Deterministic-Based Indoor Simulations

The simulations were carried out with Advanced Topographic Development & Images, "ICS Telecom" [14], a proprietary software that performs different propagation analyses. Ray-tracing methods are employed incorporating computer aided design (CAD) drawings of the indoor environment. An auxiliary software ("ICS Map Server") is used to embed the drawings converting them in a compatible digital indoor map with a spatial resolution of 0.2 m. A full wave deterministic simulation is performed launching multiple rays, taking into consideration all the relative propagation mechanisms such as diffraction, diffuse scattering, and reflection. The specific tool enables versatile and flexible simulations, including the application of different propagation models and mechanisms, and the introduction of various and complex material types, which result in the calculation of the transmission and reflection losses with significant accuracy. Furthermore, using ray-launching, it is possible to detect the angles (azimuth and elevation) of the arriving multipaths, and, thus, assess the spatial characteristics of the indoor sub-THz channel.

The Uniform Theory of Diffraction [16] is employed for the diffraction mechanism, and the modified Beckmann-Kirchhoff theory [17] is adopted for calculating diffuse scattering. This method provides an accurate approximation, considering large angles of incidence and scattering [13]. Up to fourth order reflections are taken into account during the simulations. To determine the reflection and transmission coefficients, the boundary model [18] is selected, according to which the rays are traced and refracted inside the layers of the materials.

The simulated indoor environment is illustrated in Fig. 1, where all the structures and furniture are shown, as well as the location of the transmitter (Tx) and the various receiver (Rx) positions. The green and red circles denote LOS and NLOS positions, respectively. Both Tx and Rx terminals incorporate an omnidirectional antenna (half-wave dipole), having a gain of 2.2 dBi and a half-power beamwidth (HPBW) of 78° in the elevation plane. The Tx antenna is assumed to be fixed at 1.7 m above the floor. The Tx output power is selected 0 dBm at the input of the antenna, transmitting a 4-GHz bandwidth signal, which entails a time resolution of 0.25 ns. Vertical polarization is considered. The Rx antenna is set at 1.6 m above the floor and the minimum sensitivity of the Rx is selected -150 dBm.

The external walls, indicated in Fig. 1, are made of double-sided clay bricks (9 cm), covered with plaster (2 cm) and paint (1 mm). Extruded Polystyrene (5 cm) is fixed in between. The internal walls are made of a single brick layer (9 cm) covered with plaster (2 cm) and paint (1 mm) on both sides. The rooftop is made of painted drywall panels (2 cm). The floor is made of concrete plaster (forged cement). The external windows contain double sided glass (1 cm) with 6 mm vacuum in between. The internal windows are made of 6-mm glass with 4 mm vacuum in between. The indicated partition is made of double-sided medium density fiberboard (1 cm) covered with paint (1 mm), and 2 cm air in between. To calculate the reflection and transmission coefficients, the relative refractive indexes and absorption coefficients, for all the above-mentioned materials, are taken from [19], [20]. The median values of the penetration loss for the external and internal walls are -113.1 and -64.2 dB, respectively, thus inducing heavy loss to the propagating signal at 140 GHz. However, the waves can propagate through lighter structures such as windows and partitions where lower attenuation is encountered. The median loss values for the internal windows and the partition are -15.3 and -20.1 dB, respectively. A number of 38 and 26 different Rx positions are simulated for LOS and NLOS condition, respectively.

III. Simulated Results and Analysis

The wideband simulations based on ray-tracing produce an output of power delay samples. The PDP of the channel is given by

$$P(\tau) = \sum_k a_k^2 e^{j\theta_k} \delta(\tau - \tau_k) \qquad (1)$$

where, a_k^2, τ_k, and θ_k are the power, delay, and phase samples, respectively, of the k-th multipath component, $\delta(\cdot)$ stands for the unit impulse function. During processing the PDPs are normalized to the total wideband power $P_{\text{norm}}(\tau) = P(\tau)/G$, where $G = \sum a_k^2$. Each PDP is normalized and expressed versus the excess delay. Multipath components (MPCs) that are -30 dB below the maximum, are ignored [21]. The calculated wideband parameters include the mean excess delay (m_τ) and the root-mean-square (rms) delay spread (σ_τ).

Furthermore, the maximum delay (τ_{max}) is determined that is the maximum detected path above the imposed threshold, as well as the *K*-factor (direct to multipath ratio). Details of the above-mentioned parameters and their mathematical expressions can be found in [7], [22]. Finally, the angular spread is assessed for the angle-of-arrival (AoA) of the azimuth and elevation angles of the channel (σ_φ, and σ_θ), where their definition can be found in [7], [23].

Figure 2 shows representative PDP results, derived by the simulations, for LOS and NLOS indoor locations. It is evident that the MPCs arrive at the Rx in groups (clusters), as a result of the reflected and scattered rays from the surrounding walls. The MPCs from ground and ceiling reflections arrive within the first cluster. In LOS locations there are three up to four clusters that from the PDPs, whereas in NLOS locations their number is increased varying between five and seven clusters depending on the Rx location. Furthermore, it is clear that the time delay parameters are lower in LOS locations compared with NLOS. Increased *K*-factor values are delivered in LOS locations indicating the presence of a strong LOS component. On the other hand, in NLOS positions, the attenuation of the direct path from the partitions, accounts for negative or close to zero values of *K*-factor. The existence of many strong MPCs in the late time reduces the value of *K*-factor in NLOS locations, thus implying a non-sparse channel. This is also justified by the existence of higher number of clusters, as one can observe in Fig. 2(b).

The numerical results of all the wideband parameters are listed Table I, where their statistical properties are assessed and compared with measured values available in the literature. The average simulated delay spread is found 2.4 and 10.2 ns for LOS and NLOS locations, respectively, values that are consistent with those reported in [10], [12] at 140 GHz for similar indoor LOS and NLOS environments. Furthermore, regarding only LOS conditions, the simulated delay spread values in this work are on average consistent with those found in [7], and [8], for similar indoor locations. The *K*-factor values, which are reported in [8] for LOS positions, are also comparable with the simulated values calculated in this work (9.6-17.5 dB). The average azimuth AoA spreads are found 9.6° and 6.0°, for LOS and NLOS positions, which are close to those reported in [12]. The average values obtained for the azimuth spread in [7] (8.3~12.2°), only for LOS locations, are also comparable with the above-mentioned azimuth spreads found in this work. Moreover, the average elevation AoA spread is 1.4° and 5.4°, for LOS and NLOS positions, respectively, which are comparable with the elevation spreads reported in [12], being 3.3°, for both LOS and NLOS locations. The observed discrepancies are associated to the different adopted Tx and Rx heights. The cumulative distribution functions (CDFs) of σ_τ, *K*-factor, σ_φ, and σ_θ are shown in Fig. 3. The simulated results are approximated by the Lognormal distribution. The samples include both LOS and NLOS locations.

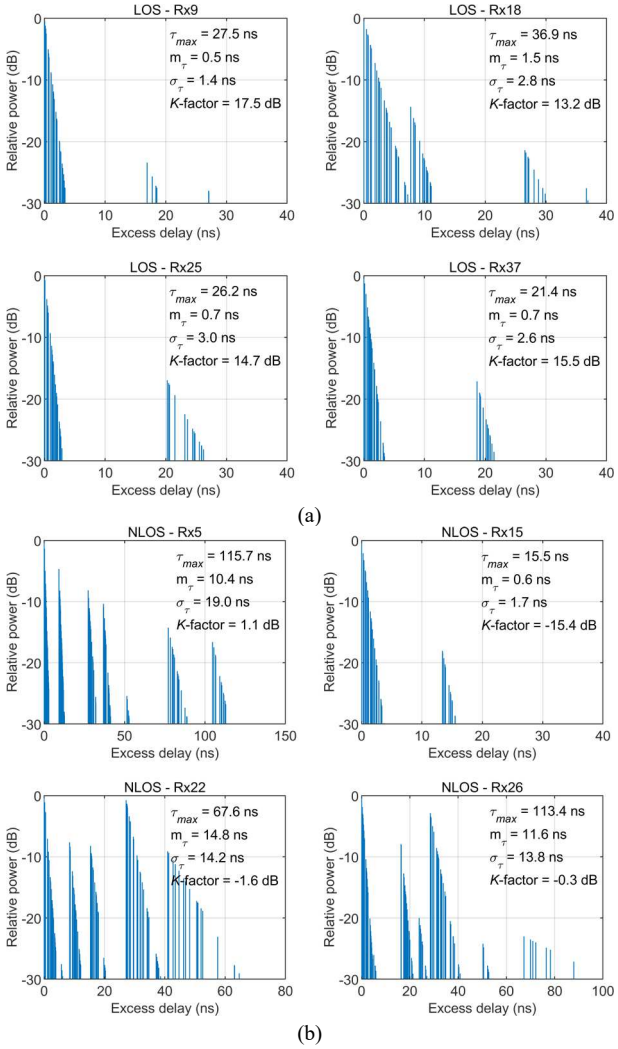

Fig. 2. Simulated power delay profiles of the indoor environment. (a) LOS locations. (b) NLOS locations.

TABLE I. TEMPORAL AND SPATIAL PROPERTIES OF THE INDOOR SIMULATED CHANNEL AT 140 GHZ.

		τ_{max} [ns]	m_τ [ns]	σ_τ [ns]	*K* [dB]	σ_φ [°]	σ_θ [°]
LOS	min	70.0	0.2	0.6	9.6	1.3	0.1
	max	123.7	1.5	5.4	17.5	25.0	1.9
	μ	95.7	0.8	2.4	13.7	9.6	1.4
	σ	12.9	0.3	1.0	2.0	4.0	0.7
NLOS	min	55.3	0.6	1.7	-15.4	5.2	4.6
	max	156.4	18.8	23.0	1.1	19.5	6.2
	μ	101.0	9.5	10.2	-5.3	6.0	5.4
	σ	44.0	4.3	6.6	5.2	1.5	0.5

Measurements

[8]: σ_τ = 1.8~5.9 ns (LOS), *K* = 8.7~25.1 dB (LOS)
[10], [12]: μ{σ_τ} = 3.0 ns (LOS), μ{σ_τ} = 9.2 ns (NLOS)
[7]: μ{σ_τ} = 4.0~5.1 ns (LOS), μ{φ_{AoA}} = 8.3~12.2° (LOS)
[12]: μ{φ_{AoA}} = 11.6° (LOS), μ{φ_{AoA}} = 5.4° (NLOS)

μ: numerical mean, σ: numerical standard deviation.

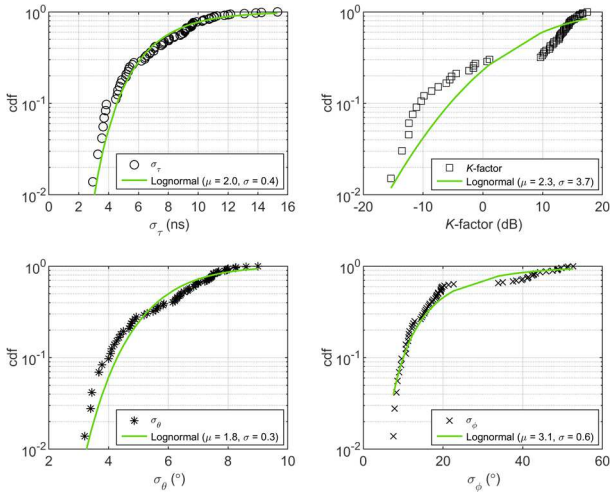

Fig. 3. Cumulative distribution functions (CDF) for the simulated parameters. The simulated data are fitted to the theoretical Lognormal distribution, considering both LOS and NLOS locations.

The results presented in Fig. 3 are in agreement with the theoretical expectations, which are also reported in [5]. The parameters (μ, σ) of the fitted Lognormal distribution are also presented in Fig. 3.

IV. Wideband Channel Modeling

The PDPs comprise clusters of MPCs that arrive at the Rx as shown in Section III and Fig. 2. Therefore, each PDP can be modeled based on the following expression

$$P(\tau) = \sum_{l=1}^{L} \sum_{k=1}^{K_l} a_{k,l}^2 e^{j\theta_{k,l}} \delta(\tau - T_l - \tau_{k,l}) \qquad (2)$$

where, a_k^2, τ_k, and θ_k denote the power, delay, and phase samples, of the k-th multipath component within cluster l. Additionally, L stands for the total number of clusters and K_l, indicates the total number of rays inside a cluster. Finally, T_l, represents the time delay of the l-th cluster and $\tau_{k,l}$ designates the delay of each k-th MPC with respect to T_l [25]. The average power of k-th ray inside the l-th cluster is given by

$$\overline{a_{k,l}^2} = \overline{a_{1,1}^2} e^{-T_l/\Gamma} e^{-\tau_{k,l}/\gamma} \qquad (3)$$

where $\overline{a_{1,1}^2}$ is the average power of the first arrived component in the first appearing cluster, and Γ, γ, represent the power decay factors of the clusters and rays, respectively [26]. Therefore, (3) is fitted to the cluster peaks in order to obtain Γ, and the rays inside each cluster to resolve γ. Converting (3) in decibels leads to the following expression

$$\overline{a_{k,l}^2} = 20\log_{10}\overline{a_{1,1}} - \left(\frac{T_l}{\Gamma} + \frac{\tau_{k,l}}{\gamma}\right) 10\log_{10}(e) \qquad (4)$$

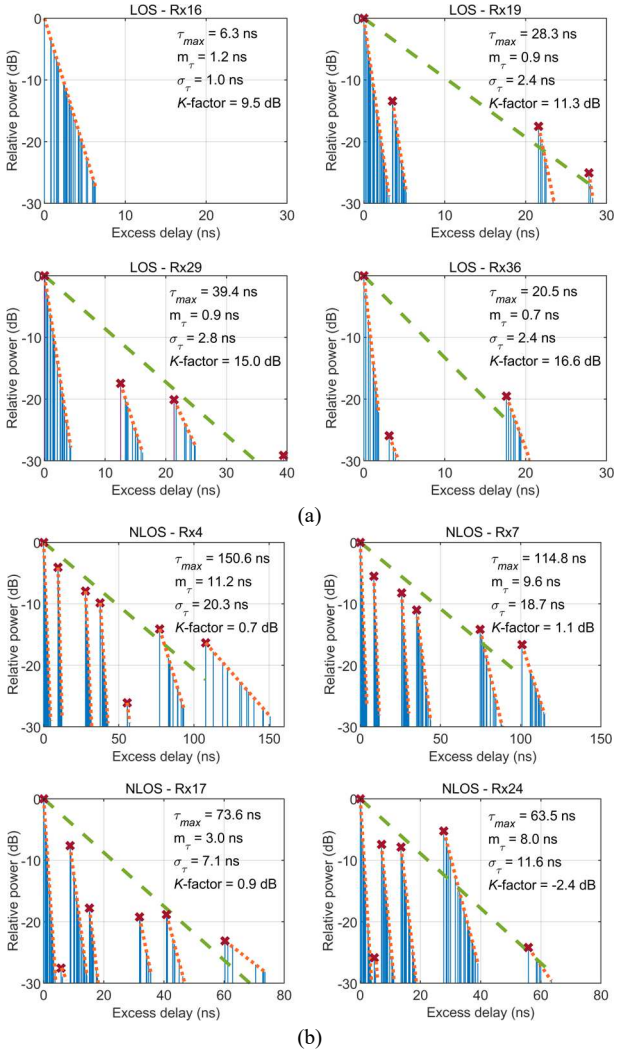

Fig. 4. Representative power delays profiles. (a) LOS locations. (b) NLOS locations. The orange dotted lines indicate the linear fit of the rays' decay inside each cluster, and the green dashed lines designate the linear fit of the clusters' decay. The purple crosses denote the cluster peaks.

where e is the exponential constant. In this regard, (4) implies a linear fit for the cluster decay, as well as for the ray decay within each cluster. Representative results are illustrated in Fig. 4, where it is shown that the introduced multi-cluster model fits very well to the simulated PDPs, in both LOS and NLOS conditions. The fitting is carried out using a linear regression. The next step is to model the interarrival times of the clusters and rays. These are assumed to arrive according to the Poisson process that is described by (5), where Λ, and λ are the cluster and ray inter-arrival times, respectively.

$$\begin{aligned} p(T_l \mid T_{l-1}) &= \Lambda e^{\Lambda(T_l - T_{l-1})} \\ p(\tau_{k,l} \mid \tau_{k-1,l}) &= \lambda e^{\lambda(\tau_{k,l} - \tau_{k-1,l})} \end{aligned} \qquad (5)$$

The calculated parameters Λ and λ of the simulated PDPs are found to approximate very well the exponential cumulative distribution function (CDF), that is analogous to the Poisson process [7]. The corresponding numerical results

of the multi-cluster model features, from all the Rx locations, are outlined in Table II. The average ray decay factor is found 1.9 and 2.5 ns for LOS and NLOS conditions, respectively. These values are very close to those modeled in [12], for similar locations (2.0 and 2.4 ns). Furthermore, the average Γ is found 4.5 and 15.6 ns, for LOS and NLOS conditions, which are comparable with the NLOS case in [12], but lower in LOS. This could be attributed to the different indoor characteristics, and dimensions. Finally, the average cluster and ray inter-arrival times are calculated 13.9 and 19.0 ns, and 1.0 and 2.5 ns, respectively. The specific results are consistent with the average values encountered in [12], where Λ^{-1} is 14.6 and 21.0 ns for LOS and NLOS positions, whereas λ^{-1}, is found 1.1 and 2.7 ns, for LOS and NLOS conditions, respectively.

TABLE II. MULTI-CLUSTER MODEL PARAMETERS AT 140 GHZ

		Λ^{-1} [ns]	λ^{-1} [ns]	Γ [ns]	γ [ns]
LOS	μ	13.9	1.0	4.5	1.9
	σ	4.1	0.3	1.6	0.7
NLOS	μ	19.0	2.5	15.6	2.5
	σ	5.5	0.6	6.8	1.0

μ: numerical mean, σ: numerical standard deviation.

V. CONCLUSION

This paper presented deterministic-based simulations in different indoor locations at 140 GHz for LOS and NLOS conditions. According to the obtained results, the indoor channel exhibited frequency selective characteristics. The obtained rms delay spread was in the range of 0.6-5.4 ns and 1.7-23.0 ns, for LOS and NLOS conditions, respectively. Furthermore, the indoor channel was modeled using a multi-cluster pattern of the MPCs that arrive in groups at the Rx. All the simulated values were found to be consistent with measured results that exist in the literature for similar indoor locations at 140 GHz. As future work the presented PDP model will be extended in the spatial domain.

REFERENCES

[1] T. S. Rappaport *et al.*, "Wireless communications and applications above 100 GHz: Opportunities and challenges for 6G and beyond," *IEEE Access*, vol. 7, pp. 78729-78757, Jun. 2019.

[2] I. F. Akyildiz, A. Kak, and S. Nie, "6G and beyond: The future of wireless communications systems," *IEEE Access*, vol. 8, pp. 133995-134030, Jul. 2020.

[3] N. Moraitis and K. S. Nikita, "Propagation study in a dense urban environment at the sub-THz band for future wireless communications," in *Proc. 17th European Conf. Antennas Propag. (EuCAP)*, Florence, Italy, Mar. 2023, pp. 1-5.

[4] Y. Xing and T. S. Rappaport, "Propagation measurement system approach at 140 GHz - Moving to 6G and above 100 GHz," in *Proc. IEEE Global Commun. Conf. (GLOBECOM)*, Abu Dhabi, United Arab Emirates, Dec. 2018, pp. 1-6.

[5] J. Gomez-Ponce *et al.*, "Directionally resolved measurement and modeling of THz band propagation channels," *IEEE Open J. Antennas Propag.*, vol. 3, pp. 663-686, Jun. 2022.

[6] M. Wang *et al.*, "Reflection characteristics measurements of indoor wireless link in D-band," *Sens.*, vol. 22, no. 18, pp. 1-16, Sep. 2022.

[7] L. Pometcu and R. D'Errico, "An indoor channel model for high data-rate communications in D-band," *IEEE Access*, vol. 8, pp. 9420-9433, Dec. 2019.

[8] Y. Chen, Y. Li, C. Han, Z. Yu, and G. Wang, "Channel measurement and ray-tracing-statistical hybrid modeling for low-THz indoor communications," *IEEE Trans. Wireless Commun.*, vol. 20, no.12, pp. 8163-8176, Dec. 2021.

[9] B. De Beelde *et al.*, "Material characterization and radio channel modeling at D-Band frequencies," *IEEE Access*, vol. 9, pp. 153528-153539, Nov. 2021.

[10] Y. Xing, T. S. Rappaport, and A. Ghosh, "Millimeter wave and sub-THz indoor radio propagation channel measurements, models, and comparisons in an office environment," *IEEE Commun. Lett.*, vol. 25, no.10, pp. 3151-3155, Oct. 2021.

[11] J. He *et al.*, "Channel measurement and path-loss characterization for low-Terahertz indoor scenarios," in *Proc. IEEE Int. Conf. Commun. Workshops (ICC Workshops)*, Montreal, QC, Canada, Jun. 2021. pp. 1-6.

[12] S. Ju *et al.*, "Millimeter wave and sub-Terahertz spatial statistical channel model for an indoor office building," *IEEE J. Sel. Areas Commun.*, vol. 39, no. 6, pp. 1561-1575, Jun. 2021.

[13] C. Han, A. O. Bicen, and I. F. Akyldiz, "Multi-ray channel modeling and wideband characterization for wireless communications in the teraherz band," *IEEE Trans. Wireless Commun.*, vol. 14, no. 5, pp. 2402-2412, May 2015.

[14] M. Z. Aslam and Y. Corre, "Simulated propagation properties for future outdoor sub-THz networks," in *Proc. IEEE 31st Int. Symp. Personal Indoor Mobile Radio Commun. (PIMRC)*, London, UK, Aug./Sep. 2021, pp. 1-6.

[15] Advanced Topographic Development & Images, "ICS Telecom - Comprehensive Network Engineering on V/U/SHF Bands," [Online]. Available: http://www.atdi.com.

[16] R. G. Kouyoumjan and P. H. Pathak, "A uniform geometrical theory of diffraction for an edge in a perfectly conducting surface," *Proc. IEEE*, vol. 42, no. 11, pp. 1148-1461, Nov.1974.

[17] H. Ragheb and E. R. Hancock, "The modified Beckmann-Kirchhoff scattering theory for rough surface analysis," *Pattern Recognit.*, vol. 40, no. 7, pp. 2004-2020, Jul. 2007.

[18] C. A. Balanis, *Advanced Engineering Electromagnetics.* 2nd ed. NJ: John Wiley & Sons Inc., 2012.

[19] R. Piesiewicz *et al.*, "Properties of building and plastic materials in the THz range," *Int. J. Infrared Millimeter Waves*, no. 28, pp. 363-371, Mar. 2007.

[20] C. Zhen and C. Jun-Cheng, "Channel characterization at 120 GHz for future indoor communication systems," *Chin. Phys. B*, vol. 22, no. 5, 2013.

[21] R. Schulpen, U. Johannsen, A. B. Smolders, and L. A. Bronckers, "Ambiguity in RMS delay spread of millimeter-wave channel measurements," in *Proc. 17th European Conf. Antennas Propag. (EuCAP)*, Florence, Italy, Mar. 2023, pp. 1-5.

[22] J. D. Parsons, *The Mobile Radio Propagation Channel*. 2nd ed. West Sussex, UK: John Wiley & Sons Ltd., 2000.

[23] A. F. Molisch, *Wireless Communications*, 2nd ed. West Sussex, UK: John Wiley & Sons Ltd., 2011.

[24] H. Mi *et al.*, "Multi-scenario millimeter wave wireless channel measurements and sparsity analysis," *China Commun.*, vol. 19, no. 11, pp. 1673-5447, Nov. 2022.

[25] A. A. M. Saleh and R. Valenzuela, "A statistical model for indoor multipath propagationm" *IEEE J. Sel. Areas Commun.*, vol. 5, no. 2, pp. 128-137, Feb. 1987.

[26] Q. H. Spenser, B. D. Jeffs, M. A. Jensen, and A. L. Swindlehurst, "Modeling the statistical time and angle of arrival characteristics of an indoor multipath channel," *IEEE J. Sel. Areas Commun.*, vol. 18, no. 3, pp. 347-360, Mar. 2000.